Hydrological effects on seismic-noise monitoring in karstic media.

C. Almagro Vidal[1], L. Zaccarelli[1], F. Pintori[1], P. L. Bragato[2], and E. Serpelloni[1]

[1]National Institute of Geophysics and Volcanology - INGV Bologna
[2]National Institute of Oceanography and Applied Geophysics - OGS

Key Points:

- Seismic ambient noise
- Seismic-noise based monitoring
- Hydrological cycle

Corresponding author: Carlos Almagro Vidal, `carlos.almagro@ingv.it`

Abstract

Fluctuations in groundwater content may produce surface deformation and affect the elastic properties of the Earth's crust. In this study we evaluate the temporal variations of the Earth's crust elastic properties (in the form of relative seismic-velocity variations) in a tectonically active region in Northern Italy characterized by the presence of karst systems. In this area, GPS measurements already revealed hydrologically-induced deformation, modulated by changes in groundwater storage. We study the relation of our seismological observations with the geodetic and hydrological results and identify the effects of groundwater-content variations in the seismic-velocity perturbations. Our results show that hydrologically-induced changes in karstic media produce significant seismic-velocity perturbations, therefore its role in tectonic-stress adjustment studies must not be ignored. Depth sensitivity analysis of our results constrain the crustal perturbations to range between 1 and 4 km depth. Results from scattering imaging locate the crustal perturbations along the main karst systems.

1 Introduction

Fluctuations in groundwater content produce changes in strain loading of the Earth's crust causing transient episodes of surface deformation that can be precisely measured by geodetic techniques (Devoti et al., 2015; Silverii et al., 2016). These surface-deformation signals have traditionally been the target of geodetic measurements to study the changes in the Earth's crust and eventually changes in groundwater. At the same time, groundwater-content variations also generate temporal alterations in the elastic properties of the subsurface. Since the propagation of seismic waves can be sensitive to the presence of fluids in the medium, seismological measurements emerge as an alternative to monitor the groundwater-content variations in the Earth's crust (Sens-Schönfelder & Wegler, 2006; Grêt et al., 2006; Voisin et al., 2016).

In order to detect transient changes in the elastic properties of the medium, the monitoring process needs uninterrupted measurements along time. One approach for continuous seismic monitoring of the Earth's crust is to exploit seismic ambient-noise cross-correlations in order to track down these medium changes in the form of relative seismic-velocity variations. This technique has been successfully applied in multiple settings: from seismogenic regions (Brenguier et al., 2008; Zaccarelli et al., 2011) to volcanic areas (Brenguier et al., 2008; Zaccarelli & Bianco, 2017). The goal of most of these applications focuses on tracking the relative seismic-velocity variations while describing any possible relation with seismogenic and/or volcanic activities. In this work however, we show that also in a tectonically active region groundwater variations can play a relevant role among the sources for seismic-velocity perturbations during seismic "quiescence" (i.e. a period without large earthquake occurrences). Noise-based monitoring has recently been applied to different areas showing the influence of groundwater-content variations (Lecocq et al., 2017; Clements & Denolle, 2018; Fores et al., 2018; Poli et al., 2020). In the case of karstic formations the hydrological-perturbation effects can be largely magnified due to their enhanced porosity and permeability, causing transient ground displacements tracked by geodetic measurements (Devoti et al., 2015; Silverii et al., 2016).

In this work we study the seismic-velocity perturbation in a karst system whose groundwater-storage dynamics and hydrologically-induced deformations have extensively been studied. It is part of the prealpine belt in the Italian Southeastern Alps (Fig. 1), located at the convergence between the Adriatic and Eurasian plates (Serpelloni et al., 2016). This area has already been the subject for tectonic deformation (Anderlini et al., 2020), hydrological cycle (Filippini et al., 2018; Grillo et al., 2019; Pintori et al., 2021), and seismicity studies (Chiaraluce et al., 2009; Anselmi et al., 2011; Danesi et al., 2015). The map in Fig. 1 shows the location of the major thrusts and fissured-karst aquifers (Bundesanstalt für Geowißenschaften und Rohstoffe, 1970) in the study area.

In this area GPS measurements show the occurrence of transient deformation episodes associated with precipitations, which are particularly evident in the *Piano del Cansiglio* (Devoti et al., 2015). Serpelloni et al. (2018) show that these hydrologically-induced deformation episodes imply sequences of extensional and compressional horizontal deformation which in turn is oriented normal to rock fractures and structural directions in karstified sectors. Fig.1 shows the horizontal strain (green arrows) at the maximum dilation stage during a hydrologically-induced deformation episode in 2010 (see Serpelloni et al., 2018), estimated by the GPS stations within a designated control area. Recently, Pintori et al. (2021), found that the transient deformation signal in the GPS displacements is highly correlated with changes in groundwater storage, and that the deformation pattern is guided by water-pressure changes in a hydrologically-active fracture, running parallel to the Cesen-Visentin fold-and-thrust belt (see Fig.1).

The aim of this work is to validate the observation of the hydrological cycle in terms of changes in the Earth's crust elastic parameters and monitor the groundwater-content variations with continuous ambient seismic noise measurements. In the first part we corroborate our results with both the estimates of watershed groundwater-content variations and with the deformation observed by GPS by using an 8-year dataset consisting of 5 stations (Fig.1, see supplementary material for more information on the data). In the following section we analyze the depth sensitivity of our results, correlate it to the geological formations, and corroborate the depth range of the groundwater-content variations. In the last part we map the lateral distribution of the seismic-velocity perturbations during a strong meteorological storm with a 4-year dataset including 10 stations (see Fig.1) and relate the result to the geomorphological characteristics of the study area.

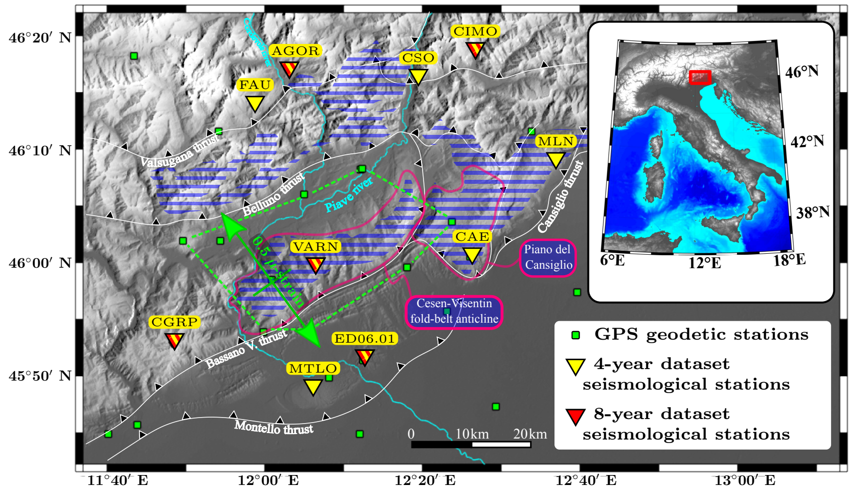

Figure 1: Location of the main faults, and the name and position of the seismic stations used for the two datasets analyzed: the 8-year long dataset of 5 stations (red triangles) and the 4-year long dataset of 10 stations (yellow triangles, see supplementary material for more information). The green squares without names are the GPS stations together with the control area (dashed green line) from previous geodetic studies. The map also shows the orientation and magnitude of the horizontal strain due to hydrologically-induced dilation during 2010 (green arrows). In striped blue, the zones identified as highly-productive aquifers with fissured karst. In the inset the location of the network in the Southeastern Alps (red frame).

2 Network response of the relative seismic-velocity variations

In this section we present the results of applying moving-window cross-spectral analysis (Clarke et al., 2011, see supplementary material for technical details) to the ambient-noise cross-correlations from the 8-year dataset (from 2011 to 2018, see Fig.1). In Fig. 2c we show the sign-reversed result of the relative seismic-velocity variations ($^{\delta v}/_{v}$) retrieved with a 30-day stack length. The colour scale shows the number of points used for the linear regression, a measure of the stability of the results (the hotter the colour, the more reliable the $^{\delta v}/_{v}$ value). For comparison, we plot the groundwater storage (GWS) variations for this area (Pintori et al., 2021) and the strain response obtained from geodetic observations (Serpelloni et al., 2018). The seismic results show a sign-reversed resemblance to both strain and GWS variations revealing an anticorrelation relation, and thus making the fluid-content variations within the karstic aquifer to be responsible for the observed seismic-velocity perturbations. Negative perturbations on $^{\delta v}/_{v}$ relate to a decrease of shear-wave velocity of the medium, which in addition coincide with GPS-observed dilation episodes; both phenomena may be explained by the increase in the amount of groundwater within the geological formation during hydrological-recharge episodes.

The agreement between the $^{\delta v}/_{v}$ result and the geodetic signal is good over the entire recording period. The mismatch of the GWS variations with the latter two is likely due to snowmelt misestimates in the hydrological model, such as the underestimate during the spring of 2014. The coherency coefficients displayed in Fig.2b indicate the reliability of the time shifts δt obtained from the cross-correlations. Periods of low coherency coefficient values may cause deviations of the $^{\delta v}/_{v}$ trend, yet the relatively high value of similarity (rarely undergoing 0.8) shows not to be the case.

Fig. 2a shows the occurrence and seismic moment released per day of the local seismicity (within a 60 km radius from the network, Romano et al., 2019). This display discards co-seismic effects as a possible source of the seismic-velocity perturbations. The relatively small strength in earthquake magnitudes (maximum $M_w = 4.4$) supports this presumption.

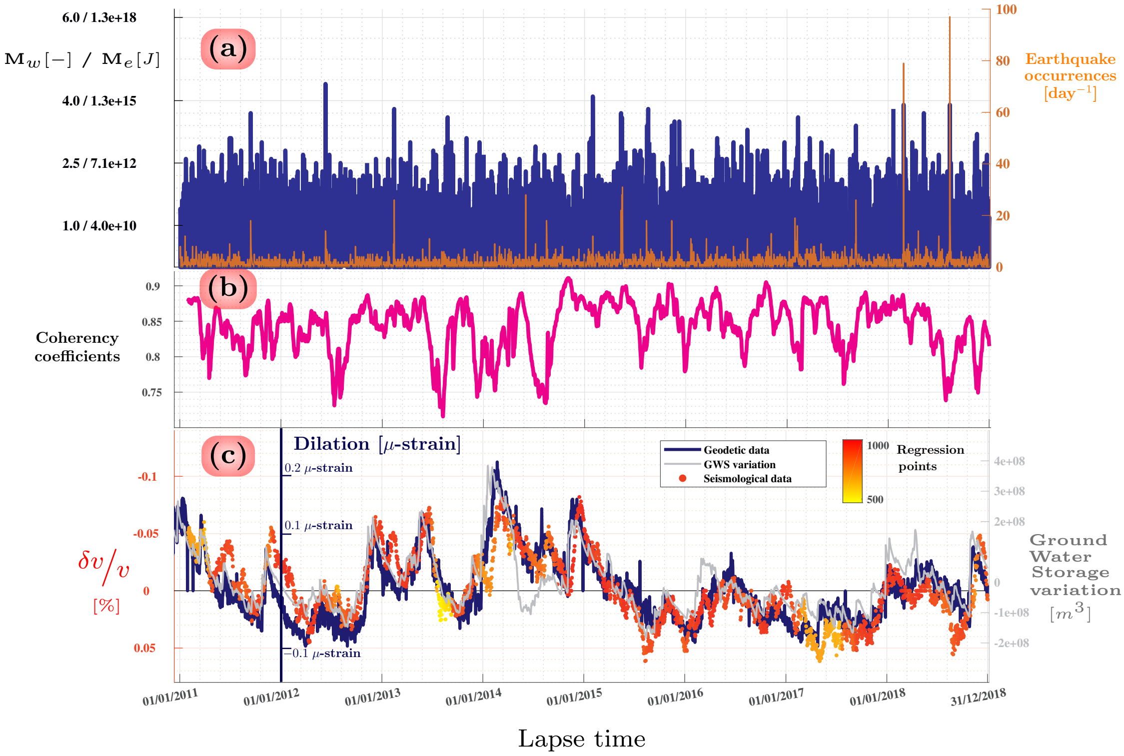

Figure 2: **(a)** Occurrence and maximum seismic moment released per day of the local seismicity during the period of study. **(b)** Averaged coherency coefficient along lapse time of the time shift estimations employed during regression. **(c)** Comparison of geodetic, hydrological and seismic noise-based monitoring observations.

3 Depth-sensitivity results

In this section we exploit the dispersive nature of the retrieved surface waves in order to constrain in depth the medium perturbations observed from our cross-correlation analysis. To that purpose, we analyze the correlation gathers in three different frequency bands in order to observe the depth sensitivity of the $^{\delta v}/_{v}$ results: $[0.1-0.3]$, $[0.4-0.6]$ and $[0.7-0.9]$ Hz.

We use the fundamental-mode sensitivity kernels of Rayleigh waves to observe the depth range where each of the frequency bands is dominant (Herrmann, 2013). We build two different 1-D geological models: one located at the middle of the hinterland basin, based on the lithostratigraphic log from well SEDICO-I (Fig. 3a.I); while the second model is representative of a site at the top of the Cesen-Visentin fold-belt anticline (see Fig.1), and it is based on the interpretation of the geological profile by the Italian Geological Survey (1992)(Fig. 3c.I). We calculate the sensitivity kernels using the depth profile and petrophysical properties of the layers defined in each of the geolithological models (Anselmi et al., 2011).

The plots in Figs. 3b.I, b.II and b.III represent the respective $^{\delta v}/_{v}$ results corresponding to the three frequency bands. Figs.3a.II and c.II show the depth-sensitivity kernels to the shear-wave velocity (β) of the corresponding frequency bands with the respective 1-D geological models on the background. Depth sensitivity curves and $^{\delta v}/_{v}$ results of the same frequency bands share the same colours (set from lower to higher frequencies: red, green and blue).

The deepest $^{\delta v}/_{v}$ result (red line), corresponding to the bottom carbonatic series (*Calcari Grigi* and *Dolomia Principale* formations) and the crystalline basement, shows no apparent relation to the hydrological result (coherency coefficient: 0.44). The $^{\delta v}/_{v}$ results from the two other frequency bands show good agreement with the groundwater storage evolution (coherency coefficients: 0.70 and 0.77, respectively), suggesting that the hydrological deformation would affect the complete karstified carbonatic sequence (*Maiolica*, *Calcari Vajont* and *Calcari Grigi* formations) along the first 3 km of crust: from 500 to 3500 m for the intermediate frequency band (green line) and from 300 to 2000 m for the highest band (blue line).

The comparison of the two higher frequency-band results reveals small variations in the depth impact of the seismic-velocity perturbation during strong storm events. During the storm episodes in November 2012 and February 2014, for example, the highest frequency result (top of the carbonatic sequence) dominates the observed $^{\delta v}/_{v}$. However, the seismic-velocity perturbations during the episodes on February 2011 and November 2018 are stronger in the intermediate frequency band, suggesting that the impact of these hydrological-recharge episodes reached the lowest section of the karstified carbonatic sequence, up to 3500 m depth.

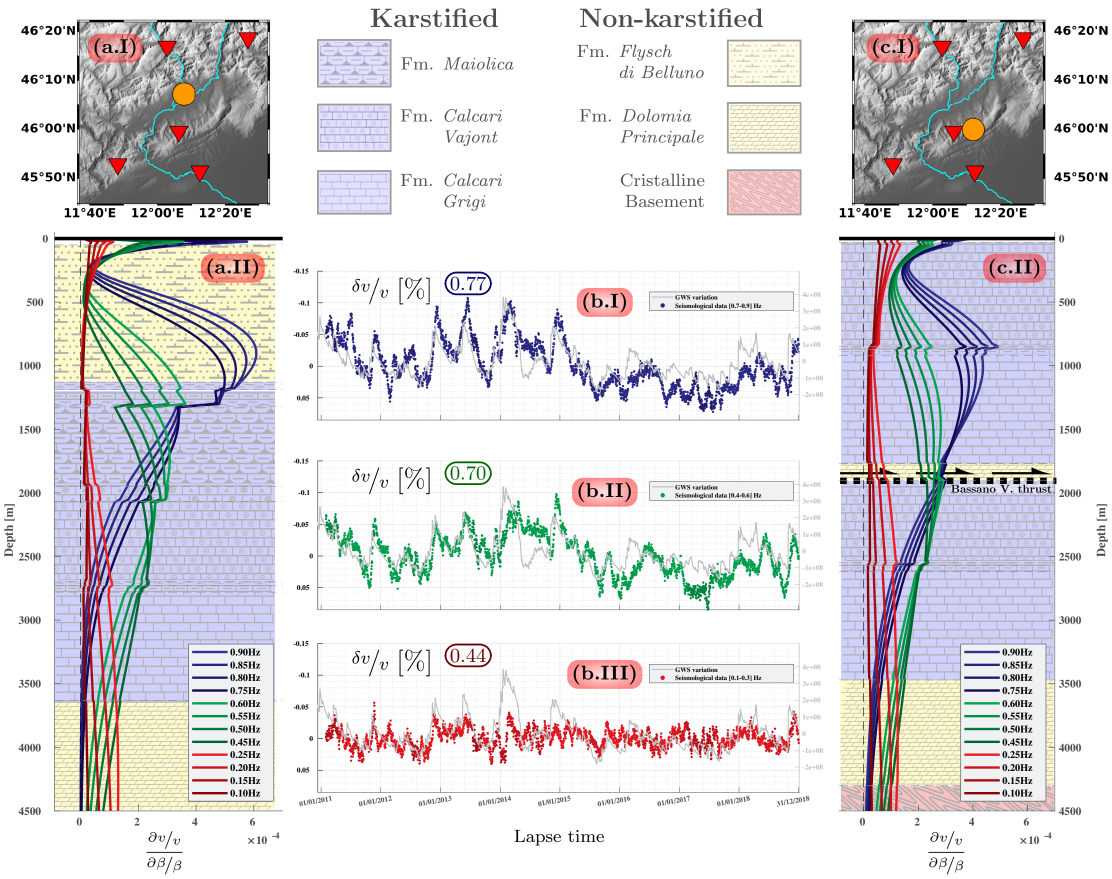

Figure 3: Depth sensitivity analysis: **(a.I)** Position of seismic stations (red triangles) and *SEDICO-I* well (orange circle) of the 1-D model. **(a.II)** Fundamental-mode Rayleigh-wave sensitivity kernel of the phase velocity to a shear-wave velocity perturbation ($\frac{\partial v/v}{\partial \beta/\beta}$) at the hinterland basin and its geological model shown in the background. **(b.I)**, **(b.II)** and **(b.III)**, the different relative seismic-velocity variation results ($\delta v/v$) obtained from the three different frequency bands of the seismic data, from top to bottom: [0.7-0.9] Hz ((b.I), blue line), [0.4-0.6] Hz ((b.II), green line), and [0.1-0.3] Hz ((b.III), red line). The gray line represents the groundwater-storage variation, same of Fig.2c. **(c.I)** and **(c.II)** Same as in (a.I) and (a.II) for the location on top of the Cesen-Visentin fold-belt anticline (orange circle in (c.I)). The legend of the main geological formations, divided according to the presence of karst as determined at the study area is displayed in the centre top.

4 Mapping results

In this section we apply a different technique based on the diffusion of the seismic scattering wavefield in order to laterally map the seismic-velocity perturbations (Pacheco & Snieder, 2005; Larose et al., 2010; Planès et al., 2015). Under the assumption that these perturbations are relatively weak, this technique applies the probability distribution of the potential scattering paths followed by the coda-wavefield arrivals through the medium in order to locate the position where perturbations occur. This methodology allows to map the perturbations by turning the radiative transfer model (Paasschens, 1997) into an imaging kernel (Obermann et al., 2013). We implement an acoustic-scattering imaging kernel based on the radiative-transfer model for 2-D isotropic media, as described in Obermann et al. (2013), and obtain a map of the ${}^{\delta v}/_{v}$ on a surface grid for every lapse time.

For this section we employ the 4-year dataset (from 2015 to 2018, see Fig.1) and focus on a particular period of abrupt increase of groundwater storage due to an exceptionally intense storm during 27-30 October 2018: *Vaia* storm (Trenti, 2018, also known as *Adrian*) Fig.4 contrasts the evolution of cumulated precipitation, horizontal ground displacements and relative seismic-velocity variation in this period. Figs.4a, 4b and 4c show the kriging result from pluviometric measurements (ARPA Veneto, 2020) at the study area prior to, during and after the *Vaia* storm, respectively. Due to the stack length of the cross-correlation gather, we use the cumulated precipitation during the previous 30 days. Fig.4e shows the horizontal ground displacements due to the hydrologically-induced deformation associated with the *Vaia* storm (Pintori et al., 2021).

Figs. 4f, 4g and 4h show the ${}^{\delta v}/_{v}$ mapping results on the same respective dates, averaged over the previous 7 days. Fig. 4d contains the time series of the seismic-velocity perturbation from the 4-year dataset and the time period corresponding to Figs. 4f, 4g and 4h. Figs. 4a and Fig. 4f show the relation between the lack of rainfall precipitation and the absence of significant seismic-velocity perturbations. Due to the lag induced by the stacking process in our seismic data, the largest amplitude of the perturbation caused by the storm is observed on later dates (see Figs. 4d and 4h). In contrast with *Vaia*-storm rainfall distribution, the seismic-velocity perturbation concentrates on the mountain belt along the central-Eastern part of the study area, corresponding to the main karst systems in the area (see Fig.1). This is in agreement with the locations where GPS stations recorded the largest displacements associated with hydrological deformation (see Fig.4e). Besides, the azimuthal-based color scale in Fig.4e shows the sense of divergence in the horizontal ground displacements (dilation) due to the water content variations following the geometry of the karstic aquifers.

It is important to emphasize from Figs. 4c and 4h that the areas with maximum precipitation do not match with the locations with the largest seismic-velocity perturbation. An explanation of this could be the different ground response to precipitations, depending on the geological formation present at the ground's surface: the sites with less permeable formations react to precipitations with efficient surface run-off and limited groundwater drainage in depth. As for the sectors consisting of karstified carbonatic formations, concentrated around the Cesen-Visentin fold belt and *Piano del Cansiglio*, water drainage is carried out more efficiently into the subsurface allowing to reach deeper aquifer levels with slight delay and loss.

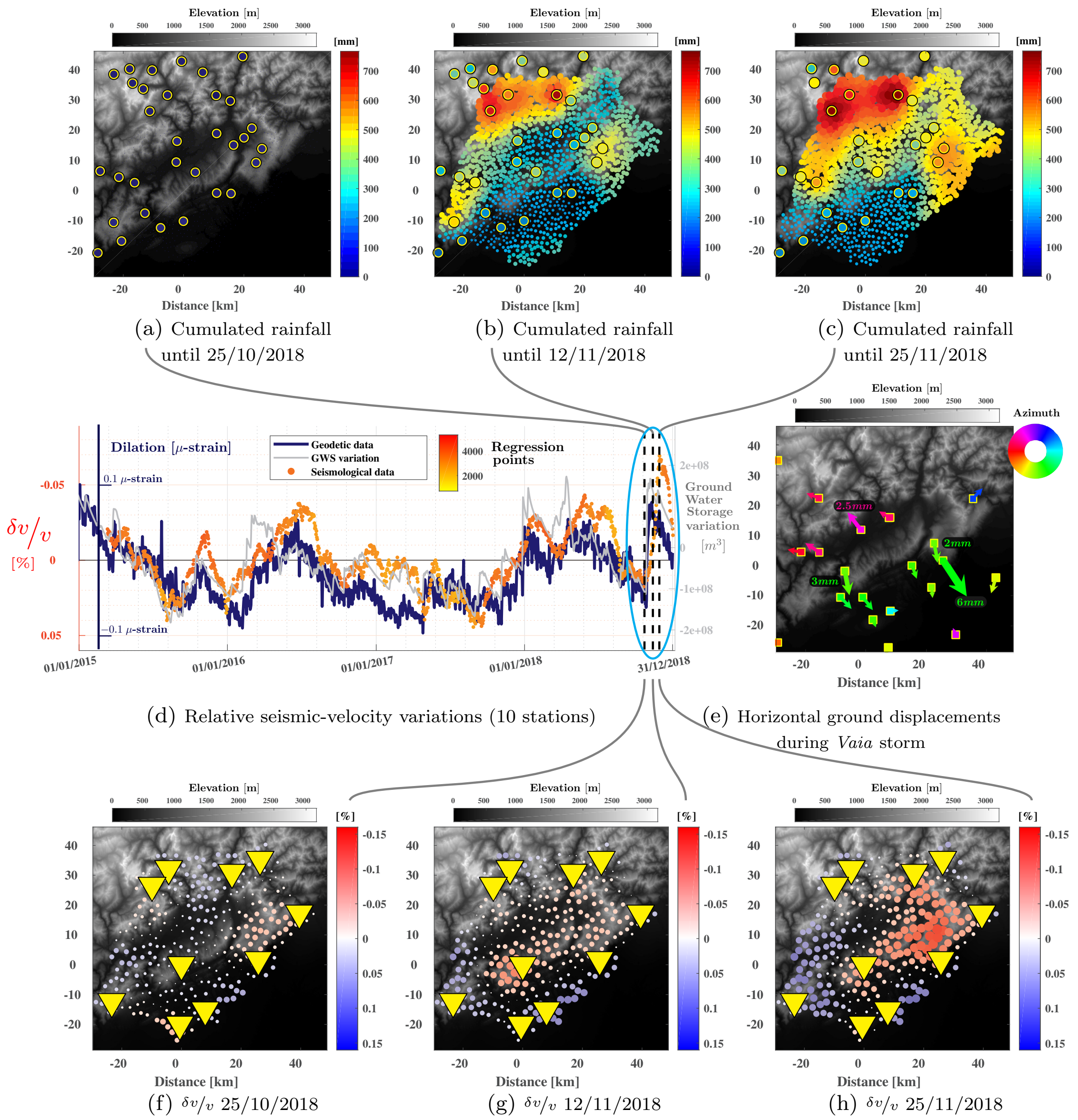

Figure 4: Relation of rainfall precipitation vs. seismic-velocity perturbation at the study area. **(a)** Kriging result from cumulated precipitation measurements from pluviometric stations (coloured circles) on 25/10/2018 over the previous 30 days. **(b)** Same as in (a), on 12/11/2018. **(c)** Same as in (a), on 25/11/2018. **(d)** Comparison between geodetic (strain) and hydrological (variation in groundwater content) observations, and the relative seismic-velocity variation at network scale obtained from the 4-year dataset. *Vaia* storm is highlighted (cyan ellipse). **(e)** Horizontal ground displacements measured at the GPS stations (coloured squares) during *Vaia* storm. **(f)** Averaged mapping result of the relative seismic-velocity variations ($\delta v/v$) with 10 stations (yellow triangles) on 25/10/2018 over the previous 7 days. **(g)** Same as in (e), on 12/11/2018. **(h)** Same as in (e), on 25/11/2018.

5 Discussion

In this study, the temporal evolution of $^{\delta v}/_{v}$ measurements match the strain evolution observed in the area and explained through hydrological modelling of water-content variations. According to the depth-sensitivity analysis, the observed hydrological variations affect crustal levels deeper than described in similar studies (Lecocq et al., 2017; Clements & Denolle, 2018). Although we consider that the depths reached by the seismic-velocity perturbations was possible because of the geological characteristics and dimensions of the aquifer system, we consider that this depth range might not be limited to karst systems but could extend to different geological settings (Wang et al., 2017; Poli et al., 2020). Besides, the depth levels that our $^{\delta v}/_{v}$ result represents correspond to the top seismogenic depth range in the area (from 3 to 4 km depth, Romano et al., 2019). This feature can confirm the role that hydrological-loading variations can play in stress control for deeper seismogenic levels in this study area (Pintori et al., 2021).

The use of ambient-noise cross-correlation analysis for monitoring seismic-velocity changes has increased in popularity in the foretelling of volcanic eruptions (Brenguier et al., 2008) which in turn motivates the application of this technique in the study of earthquake preparatory phases. In this case we show that hydrological processes generate seismic-velocity perturbations of such large mangitudes that can lead to misinterpretations especially before earthquake occurrences. Therefore, seismic studies regarding key inferences on the tectonic-stress adjustments must correct for the hydrological effects, and could profit from geodetic measurements and hydrological modelling in order to quantify them (Sens-Schönfelder & Wegler, 2006; Rivet et al., 2015; Budi-Santoso & Lesage, 2016; Wang et al., 2017).

The application of imaging techniques can lead to a better understanding of karst-aquifer structure and dynamics. In our study we obtained mapping results of the seismic-velocity perturbation in agreement with the geological structure of the study area yet employing a simple imaging kernel: considering the scattering properties as being homogeneous throughout the medium is a rather delicate assumption. A more accurate approach implies the use of scattering imaging kernels for inhomogeneous media in order to account for the lateral geological variations of the study area.

6 Conclusions

Ambient noise has been successfully employed to monitor groundwater content variations in a tectonically active area. Our analysis confirmed the identification of transient variations in the crust's elastic properties that are not related to local seismicity or other tectonic processes (e.g. aseismic deformation). Geodetic and hydrological observations confirm that the seismic-velocity perturbations are caused by the recharge/discharge cycles in the karstic aquifers. Moreover, we constrained the depth range of the hydrologically-induced perturbation to the carbonatic formations (within the first 4 km of depth). The spatial distribution of the main ${}^{\delta v}/_{v}$ variations may not correspond to the major rainfall locations suggesting that geological formations at the surface play a relevant role in the ${}^{\delta v}/_{v}$ response to hydrological loading, especially karstified formations.

Acknowledgments

This research is financially supported by the Project “Transient of strain and stress experiment in Italy (TRANSIENTI)”, funded by the Italian Ministry of Education, University and Research (MIUR). The seismic data used for this work are freely available at the OGS Archive System of Instrumental Seismology - OASIS (Priolo et al., 2015; Working Group OASIS, 2011). We appreciate Dr. L. Anderlini for fruitful discussions that contributed to this paper.

References

Anderlini, L., Serpelloni, E., Tolomei, C., Martini, P. M. D., Pezzo, G., Gualandi, A., & Spada, G. (2020). New insights into active tectonics and seismogenic potential of the Italian Southern Alps from vertical geodetic velocities. *Solid Earth Discussions*, 1–27. doi: 10.5194/se-2020-10

Anselmi, M., Govoni, A., De Gori, P., & Chiarabba, C. (2011). Seismicity and velocity structures along the South-Alpine thrust front of the Venetian Alps (NE-Italy). *Tectonophysics*, *513*(1-4), 37–48. doi: 10.1016/j.tecto.2011.09.023

ARPA Veneto. (2020). *Dati meteorologici di precipitazione: 2011-2018.* Sistema Nazionale per la Protezione dell’Ambiente. Retrieved from `www.arpa.veneto.it/bollettini/storico/Mappa_2020_PREC.htm?t=RG`

Brenguier, F., Campillo, M., Hadziioannou, C., Shapiro, N., Nadeau, R., & Larose, E. (2008). Postseismic relaxation along the San Andreas Fault at Parkfield from continuous seismological observations. *Science*, *321*(5895), 1478–1481. doi: 10.1126/science.1160943

Brenguier, F., Shapiro, N., Campillo, M., Ferrazzini, V., Duputel, Z., Coutant, O., & Nercessian, A. (2008). Towards forecasting volcanic eruptions using seismic noise. *Nature Geoscience*, *1*(2), 126–130. doi: 10.1038/ngeo104

Budi-Santoso, A., & Lesage, P. (2016, 04). Velocity variations associated with the large 2010 eruption of Merapi volcano, Java, retrieved from seismic multiplets and ambient noise cross-correlation. *Geophysical Journal International*, *206*(1), 221-240. Retrieved from `https://doi.org/10.1093/gji/ggw145` doi: 10.1093/gji/ggw145

Bundesanstalt für Geowißenschaften und Rohstoffe. (1970). *International Hydrogeological Map of Europe: Sheet C5 Bern 1:1 500 000.* Bundesanstalt für Bodenforschung/UNESCO. Retrieved from `www.bgr.bund.de/ihme1500`

Chiaraluce, L., Valoroso, L., Anselmi, M., Bagh, S., & Chiarabba, C. (2009). A decade of passive seismic monitoring experiments with local networks in four Italian regions. *Tectonophysics*, *476*(1-2), 85–98. doi: 10.1016/j.tecto.2009.02.013

Clarke, D., Zaccarelli, L., Shapiro, N., & Brenguier, F. (2011). Assessment of resolution and accuracy of the moving window cross spectral technique for monitoring crustal temporal variations using ambient seismic noise. *Geophysical Journal International*, *186*(2), 867–882. doi: 10.1111/j.1365-246X.2011.05074.x

Clements, T., & Denolle, M. A. (2018). Tracking groundwater levels using the ambient seismic field. *Geophysical Research Letters*, *45*(13), 6459–6465. doi: 10.1029/2018GL077706

Danesi, S., Pondrelli, S., Salimbeni, S., Cavaliere, A., Serpelloni, E., Danecek, P., ... Massa, M. (2015). Active deformation and seismicity in the Southern Alps (Italy): The Montello hill as a case study. *Tectonophysics*, *653*, 95–108. doi: 10.1016/j.tecto.2015.03.028

Devoti, R., Zuliani, D., Braitenberg, C., Fabris, P., & Grillo, B. (2015). Hydrologically induced slope deformations detected by GPS and clinometric surveys in the Cansiglio Plateau, Southern Alps. *Earth and Planetary Science Letters*, *419*, 134–142. doi: 10.1016/j.epsl.2015.03.023

Filippini, M., Squarzoni, G., De Waele, J., Fiorucci, A., Vigna, B., Grillo, B., … others (2018). Differentiated spring behavior under changing hydrological conditions in an alpine karst aquifer. *Journal of hydrology*, *556*, 572–584. doi: 10.1016/j.jhydrol.2017.11.040

Fores, B., Champollion, C., Mainsant, G., Albaric, J., & Fort, A. (2018). Monitoring saturation changes with ambient seismic noise and gravimetry in a karst environment. *Vadose Zone Journal*, *17*(1), 1–12. doi: 10.2136/vzj2017.09.0163

Grêt, A., Snieder, R., & Scales, J. (2006). Time-lapse monitoring of rock properties with coda wave interferometry. *Journal of Geophysical Research: Solid Earth*, *111*(B3). doi: 10.1029/2004JB003354

Grillo, B., Braitenberg, C., Nagy, I., Devoti, R., Zuliani, D., & Fabris, P. (2019). Cansiglio karst plateau: 10 years of geodetic–hydrological observations in seismically active Northeast Italy. In *Geodynamics and earth tides observations from global to micro scale* (pp. 171–187). Springer. doi: 10.1007/s00024-018-1860-7

Herrmann, R. B. (2013). Computer programs in seismology: An evolving tool for instruction and research. *Seismological Research Letters*, *84*(6), 1081–1088. doi: 10.1785/0220110096

Italian Geological Survey. (1992). *Carta Geologica: Belluno (Foglio 063, 1:50 000).* Organo Cartografico dello Stato, Istituto Poligrafico e Zecca dello Stato, Roma.

Larose, E., Planes, T., Rossetto, V., & Margerin, L. (2010). Locating a small change in a multiple scattering environment. *Applied Physics Letters*, *96*(20), 204101. doi: 10.1063/1.3431269

Lecocq, T., Longuevergne, L., Pedersen, H. A., Brenguier, F., & Stammler, K. (2017). Monitoring ground water storage at mesoscale using seismic noise: 30 years of continuous observation and thermo-elastic and hydrological modeling. *Scientific reports*, *7*(1), 1–16. doi: 10.1038/s41598-017-14468-9

Obermann, A., Planes, T., Larose, E., & Campillo, M. (2013). Imaging preeruptive and coeruptive structural and mechanical changes of a volcano with ambient seismic noise. *Journal of Geophysical Research: Solid Earth*, *118*(12), 6285–6294. doi: 10.1002/2013JB010399

Paasschens, J. (1997). Solution of the time-dependent Boltzmann equation. *Physical Review E*, *56*(1), 1135. doi: 10.1103/PhysRevE.56.1135

Pacheco, C., & Snieder, R. (2005). Time-lapse travel time change of multiply scattered acoustic waves. *The Journal of the Acoustical Society of America*, *118*(3), 1300–1310. doi: 10.1121/1.2000827

Pintori, F., Serpelloni, E., Longuevergne, L., Garcia-Aristizabal, A., Belardinelli, M. E., Faenza, L., … Gualandi, A. (2021). Remote hydrological control on crustal seismicity. *Journal of Geophysical Research: Solid Earth*, *126*. doi: 10.1029/2020JB020586

Planès, T., Larose, E., Rossetto, V., & Margerin, L. (2015). Imaging multiple local changes in heterogeneous media with diffuse waves. *The Journal of the Acoustical Society of America*, *137*(2), 660–667. doi: 10.1121/1.4906824

Poli, P., Marguin, V., Wang, Q., D'Agostino, N., & Johnson, P. (2020). Seasonal and coseismic velocity variation in the region of L'Aquila from single station measurements and implications for crustal rheology. *Journal of Geophysical Research: Solid Earth*, *125*(7), e2019JB019316. doi: 10.1029/2019JB019316

Priolo, E., Laurenzano, G., Barnaba, C., Bernardi, P., Moratto, L., & Spinelli, A. (2015). OASIS: The OGS Archive System of Instrumental Seismology. *Seismological Research Letters*, *86*(3), 978–984. doi: 10.1785/0220140175

Rivet, D., Brenguier, F., & Cappa, F. (2015). Improved detection of preeruptive seismic velocity drops at the Piton de La Fournaise volcano. *Geophysical Research Letters*, *42*(15), 6332–6339. doi: 10.1002/2015GL064835

Romano, M. A., Peruzza, L., Garbin, M., Priolo, E., & Picotti, V. (2019). Microseismic portrait of the Montello thrust (Southeastern Alps, Italy) from a dense high-quality seismic network. *Seismological Research Letters*, *90*(4), 1502–1517. doi: 10.1029/2006GL027797

Sens-Schönfelder, C., & Wegler, U. (2006). Passive image interferometry and seasonal variations of seismic velocities at Merapi volcano, Indonesia. *Geophysical research letters*, *33*(21). doi: 10.1029/2006GL027797

Serpelloni, E., Pintori, F., Gualandi, A., Scoccimarro, E., Cavaliere, A., Anderlini, L., … Todesco, M. (2018). Hydrologically induced karst deformation: Insights from GPS measurements in the Adria-Eurasia plate boundary zone. *Journal of Geophysical Research: Solid Earth*, *123*(5), 4413–4430. doi: 10.1002/2017JB015252

Serpelloni, E., Vannucci, G., Anderlini, L., & Bennett, R. A. (2016). Kinematics, seismotectonics and seismic potential of the Eastern sector of the European Alps from GPS and seismic deformation data. *Tectonophysics*, *688*, 157–181. doi: 10.1016/j.tecto.2016.09.026

Silverii, F., d'Agostino, N., Métois, M., Fiorillo, F., & Ventafridda, G. (2016). Transient deformation of karst aquifers due to seasonal and multiyear groundwater variations observed by GPS in Southern Apennines (Italy). *Journal of Geophysical Research: Solid Earth*, *121*(11), 8315–8337. doi: 10.1002/2016JB013361

Trenti, A. (2018). *Perturbazione eccezionale del 27–29 ottobre 2018, Trento, 16 November 2018.* Provincia Autonoma di Trento.

Voisin, C., Garambois, S., Massey, C., & Brossier, R. (2016). Seismic noise monitoring of the water table in a deep-seated, slow-moving landslide. *Interpretation*, *4*(3), SJ67–SJ76. doi: 10.1190/INT-2016-0010.1

Wang, Q.-Y., Brenguier, F., Campillo, M., Lecointre, A., Takeda, T., & Aoki, Y. (2017). Seasonal crustal seismic velocity changes throughout Japan. *Journal of Geophysical Research: Solid Earth*, *122*(10), 7987–8002. doi: 10.1002/2017JB014307

Working Group OASIS. (2011). *The OGS Archive System of Instrumental Seismology.* OGS. Retrieved from `http://oasis.crs.inogs.it`

Zaccarelli, L., & Bianco, F. (2017). Noise-based seismic monitoring of the Campi Flegrei caldera. *Geophysical Research Letters*, *44*(5), 2237–2244. doi: 10.1002/2016GL072477

Zaccarelli, L., Shapiro, N., Faenza, L., Soldati, G., & Michelini, A. (2011). Variations of crustal elastic properties during the 2009 L'Aquila earthquake inferred from cross-correlations of ambient seismic noise. *Geophysical research letters*, *38*(24). doi: 10.1029/2011GL049750